JACS
JOURNAL OF THE AMERICAN CHEMICAL SOCIETY

Communication

pubs.acs.org/JACS

Colloidal Synthesis of Quantum Confined Single Crystal $CsPbBr_3$ Nanosheets with Lateral Size Control up to the Micrometer Range

Javad Shamsi,[†,§] Zhiya Dang,[†] Paolo Bianchini,[‡] Claudio Canale,[‡] Francesco Di Stasio,[†] Rosaria Brescia,[†] Mirko Prato,*[,†] and Liberato Manna*[,†]

[†]Nanochemistry Dept., Istituto Italiano di Tecnologia, Via Morego 30, 16163 Genova, Italy

[§]Dipartimento di Chimica e Chimica Industriale, Università degli Studi di Genova, Via Dodecaneso 31, 16146 Genova, Italy

[‡]Nanophysics Dept., Istituto Italiano di Tecnologia, Via Morego 30, 16163 Genova, Italy

Supporting Information

ABSTRACT: We report the nontemplated colloidal synthesis of single crystal $CsPbBr_3$ perovskite nanosheets with lateral sizes up to a few micrometers and with thickness of just a few unit cells (i.e., below 5 nm), hence in the strong quantum confinement regime, by introducing short ligands (octanoic acid and octylamine) in the synthesis together with longer ones (oleic acid and oleylamine). The lateral size is tunable by varying the ratio of shorter ligands over longer ligands, while the thickness is mainly unaffected by this parameter and stays practically constant at 3 nm in all the syntheses conducted at short-to-long ligands volumetric ratio below 0.67. Beyond this ratio, control over the thickness is lost and a multimodal thickness distribution is observed.

The rise of graphene[1] has ignited global interest in noncarbon-based ultrathin two-dimensional (2D) nanomaterials, such as transition metal dichalcogenides, layered metal oxides, and hexagonal boron nitride, to name a few.[2] Several synthetic methods have been developed for the preparation of 2D nanomaterials,[2a] including bottom-up wet chemistry routes. The latter have rapidly evolved to the point that they can now deliver 2D nanostructures also for nonlayered materials, such as noble metals, metal oxides, and metal chalcogenides.[3] These 2D nanomaterials offer unique advantages over their 3D counterparts, in addition to the increased specific surface area. In particular, 2D colloidal semiconductor nanocrystals exhibit remarkable optical properties:[4] their absorption edges and the emission spectra are narrow (even below 10 nm at room temperature), their photoluminescence quantum yield (PLQY) is typically high, in the 30−80% range, and their PL lifetimes are usually fast, making them good candidates for light emission applications.[4b] These optical properties are strictly dependent on the sheet/platelet thicknesses, which can be finely tuned in colloidal synthesis by a proper choice of the organic surfactants that are used to control the growth.

Lead halide based perovskites obtained by reliable colloidal synthesis approaches have emerged as promising materials for solution-processable photovoltaic technology in the past two years.[5] When seeking for a synthesis route to prepare nanoplatelets or nanosheets of a nonlayered material, it is critical to break the crystal symmetry and promote anisotropic growth. In the case of organic−inorganic hybrid perovskite, so far three works have addressed the colloidal synthesis of $MAPbBr_3$ (MA = methylammonium) nanoplatelets (NPLs) with confined thickness,[5f,6] while in another work $(C_4H_9NH_3)_2PbBr_4$ nanosheets were directly grown on a SiO_2/Si substrate and then detached from the substrate and suspended in solution.[7] Several reports have dealt with shape control in the colloidal synthesis of fully inorganic $CsPbX_3$ (X being a halide) nanocrystals. Zhang et al. observed the evolution of $CsPbX_3$ (X = Br, I) nanocubes to nanowires (NWs) by increasing the reaction time from few seconds up to 60 min in a synthesis that was initially used to prepare nanocubes.[8] At a reaction time around 30 min, the sample consisted of a mixture of NWs and square-shaped nanosheets (NSs) of 100 nm lateral dimensions. Sun et al. reported shape control of $CsPbX_3$ perovskite via a reprecipitation process at room temperature, which yielded green emitting NPLs/NSs with edge length of around 100 nm.[9] Recently, two colloidal routes were reported on the anisotropic growth of all-inorganic $CsPbBr_3$ NPLs exhibiting a strong 2D confinement of the carriers.[10] In one of them, our group devised a room temperature synthesis to $CsPbBr_3$ NPLs with monolayer-level thickness control in the 3−5 unit cells range.[10a] In the other work, Bekenstein et al.[10b] observed that the procedure to prepare $CsPbBr_3$ nanocubes,[5b] when carried out at temperatures in the 90−130 °C range, yields NPLs. In the same synthesis scheme, no particles were formed at temperatures as low as 70 °C, while at 150 °C nanocubes were synthesized. The prepared NPLs could then undergo lateral oriented attachment, forming nanosheets (NSs) with lateral size up to 200 nm.

We show here an approach for the synthesis of colloidal orthorhombic $CsPbBr_3$ NSs with thickness in the range of 2−3 unit cells (i.e., around 3 nm) and with lateral dimensions from 300 nm up to a few micrometers. The process is carried out using standard air-free techniques and is an evolution of the synthesis reported by Protesescu et al.[5b] Our major change is to use Cs-oleate dissolved in oleic acid (OlAc) instead of octadecene (as done instead in the work of Protesescu et al.). This change alone leads to NPLs and not to cubes, over a wide temperature range (from 50 to 150 °C, see Figure S1 of the Supporting Information (SI)), differently from Bekenstein et al., who could get NPLs only in a narrower temperature range (see above).[10b] In our initial

Received: March 27, 2016
Published: May 26, 2016

DOI: 10.1021/jacs.6b03166
J. Am. Chem. Soc. 2016, 138, 7240−7243

Table 1. Reaction Conditions for the Synthesis of NSs with Various Lateral Sizes and Summary of the Relevant Geometrical and Optical Properties: Average Size, Half Width at Half-Maximum (HWHM) of the Size Distribution, PL Wavelength, and Estimated Thickness[a]

OctAc volume (= OctAm volume)	short/long ligands volumetric ratio (X)	NS ⟨size⟩ (nm)/size distribution HWHM (nm)	PL (nm) (±2 nm)	estimated thickness[9] from PL position
250 μL	0.33	280/120	452	2.7 nm
300 μL	0.40	610/120	458	2.9 nm
400 μL	0.52	975/200	458	2.9 nm
500 μL	0.67	5160/1300	458; 491	2.9 nm; 4 nm

[a]In all reactions, 250 μL of OlAc and 250 μL of OlAm are used as long chain ligands. An additional 1 mL of OlAc is added with the Cs precursor.

scheme, tuning of the lateral size of the NPLs (from 50 to 200 nm, see Figure S2) was possible by varying the reaction time (from a few seconds up to a few minutes). However, the NPLs would grow in thickness as well, as their PL emission shifted from 450 nm (compatible with a thickness of approximately 2.5 nm, as calculated with the empirical formula by Sun et al.[9]), to 510−520 (compatible with a thickness of 4.6−4.9 nm, therefore out of the strong confinement regime) and led to a multimodal thickness distribution (Figure S2).

A second change in the synthesis was to introduce shorter ligands (in addition to oleic acid, OlAc, and oleylamine, OlAm, of the standard protocol), namely, octanoic acid (OctAc) and octylamine (OctAm). By varying the ratio of these two short ligands over that of the longer ligands (OlAc and OlAm), we could control the lateral size of the particles, which could be tuned from 300 nm up to 5 μm (with a higher ratio of short to long ligands yielding larger nanosheets), while at the same time the thickness remained fixed at 2−3 unit cells (2.5−3 nm, see Table 1). The use of short ligands therefore enabled the synthesis of NSs with large lateral dimensions and in which the vertical dimension was always in the strong quantum confinement regime. Although OctAc alone could be used as short ligand to promote the lateral growth of the sheets (see Figure S3A), in that case the quality of the NSs, in terms of lateral size distribution, was not as good as when OctAm was added to OctAc. However, when using OctAm alone as a short ligand, no sheets were obtained but only a mixture of large crystals and thin NPLs/NSs (see Figure S3B). Therefore, the use of both short ligands in conjunction was necessary. Similar results were found when working with nonanoic acid instead of OctAc (data not shown).

Other parameters that were found critical in controlling the shape and the thickness of the sheets were the temperature and the reaction time. The optimal temperature range for growth was 145−155 °C. Temperatures above 155 °C led to sheets with an addition of various byproducts (including cubes), whereas below 145 °C the growth was slow and the shape of the NSs was not regular, with nonsharp edges (see Figure S4 of the SI). The optimal growth time was up to 5 min. Attempts to grow larger sheets by increasing the reaction time resulted in aggregation of the particles. Therefore, lateral size control was best achieved by tuning the ratio of short to long ligands rather than by increasing the reaction time over 5 min. The role of OlAc and of the short ligands in promoting NS growth and in fine-tuning the lateral size, and especially in depressing the growth rate in the vertical direction, is presently unclear and will require further scrutiny. The marked instability of the early aliquots from the synthesis under the electron beam of the TEM made it difficult to perform detailed structural and morphological analyses on them, and therefore to advance solid hypotheses on the growth mechanism (whether this proceeds by oriented attachment or by addition of monomers to initially formed nuclei).

Typical (TEM) images of the NSs prepared at different short to long ligand volumetric ratios (henceforth defined as "X") are reported in Figure 1, along with histograms of lateral size

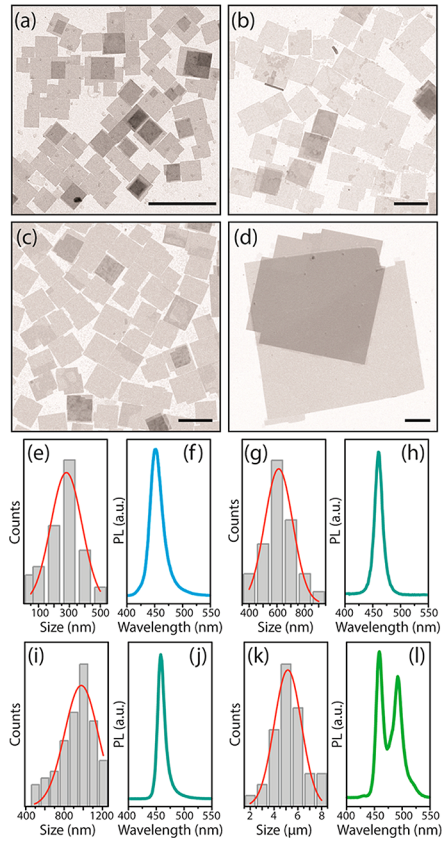

Figure 1. Effect of increasing the ratio of short to long ligands on controlling the lateral size of $CsPbBr_3$ NSs. Representative (a−d) TEM images, (e,g,i,k) lateral size distribution, and (f,h,j,l) emission spectra of $CsPbBr_3$ NSs prepared with short-to-long ligands molar ratios equal to X = 0.33 (a,e,f), X = 0.40 (b,g,h), X = 0.52 (c,i,j), and X = 0.67 (d,k,l). Scale bars in all TEM images are 1 μm long.

distributions and PL spectra. Corresponding absorption spectra are reported in Figure S6. In all cases, the shapes of the NSs were roughly squared and with sharp edges, supporting a single crystalline nature for each of them. The NSs synthesized when working at X = 0.33 (see Figure 1a) exhibited a quite broad lateral size distribution, centered ∼ 280 nm (Figure 1e and Table 1, where the average size is reported together with the half width at half-maximum, HWHM, of the size distribution, as obtained via Gaussian fit of the size distribution histogram) and a narrow PL spectrum centered at 452 nm. This emission wavelength, compared with that of 8.5 nm cube-shaped NCs (emitting at approximately 510 nm),[11] indicates that the thickness of our NSs

DOI: 10.1021/jacs.6b03166
J. Am. Chem. Soc. 2016, 138, 7240−7243

should be below the Bohr exciton diameter for $CsPbBr_3$, i.e., below 7 nm.[5b] A thickness of 2.7 nm could be estimated using the Sun formula.[9] This value seems quite reliable since in our previous work we had observed a similar emission wavelength for quantum confined $CsPbBr_3$ NPLs having thicknesses of 2.5 nm.[10a] The presence of a single emission peak suggests that, in spite of the relatively broad lateral size distribution, our NSs had a narrow thickness distribution. By increasing the X ratio up to 0.4 and 0.52, the average lateral size of the NSs increased to 610 nm (Figure 1b, 1g) and to 975 nm (Figure 1c, 1i), respectively. In both cases, the lateral size distribution was still quite broad (Table 1); however, the PL spectrum was narrow and centered at ~458 nm (Figure 1h,j), matching the PL emission wavelength of 3 nm thick $CsPbBr_3$ NPLs.[10a] In particular, the sample prepared at X = 0.52 exhibited a narrow emission peak, with full width at half-maximum of 13 nm, indicating a unimodal distribution of thicknesses (Figure 1j). Further increasing of the amount of short ligands in the solution (X = 0.67) led to large nanosheets, with mean lateral size of 5.16 μm (Figure 1d,k, Table 1), but with poor control over the thickness, as seen by the multiple peaks in the emission spectrum (with two distinct maxima at 458 and 491 nm, Figure 1l), indicating a roughly bimodal thickness distribution.

Our analysis focused then on the synthesis that delivered the sample characterized by the narrower thickness distribution coupled with a mean lateral size around 1 μm, i.e., the one prepared at X = 0.52 (Figure 1c,i,j). For this sample, we measured a PL quantum yield (QY) of ~33%, which is higher than that of bulk $CsPbBr_3$.[12] The increased PLQY could be related to a quantum confinement effect, although it might simply be due to a lower density of trap states in the NSs compared to the bulk case. We also recorded the PL lifetime at the PL peak value (λ_{PL} = 456 nm, see Figure S7 of the SI). Similar to the $CsPbBr_3$ nanoplatelets reported by Sun et al.,[9] a three-exponential function was necessary to fit the PL decay. The estimated average PL lifetime (τ) was of 4.3 ns, in line with previously published values for $CsPbBr_3$ NPLs[10a] (τ = 3 ns) or for $(C_4H_9NH_3)_2PbBr_4$ NSs[7] (τ = 1.61 ns) synthesized with different methods. The overall PL lifetime falls within the range of perovskite NCs with shapes differing from sheets or platelets, for example, the cubic $CsPbX_3$ (where X = Br or I, τ = 1- 22 ns) NCs that were recently employed as gain material in lasers.[13]

Figure 2a reports a confocal microscopy image of the NSs, recorded by exciting the sample with a pulsed laser (LDH-D-C-405, PicoQuant GmbH, Berlin, Germany) at 405 nm and with a 40 MHz repetition rate. The emission from the NSs was collected over two channels, one in the 425−475 nm spectral window, which corresponds to the spectral emission range of the sample in solution (coded in blue), and the other channel in the 500−550 nm spectral window, centered at around the emission wavelength of bulk $CsPbBr_3$[10a] (coded in green). Apart from a few byproducts emitting in the green channel, all the NSs were emitting in the blue channel, which corroborates the narrow thickness distribution of the sheets. Atomic force microscopy (AFM) was used to evaluate the thickness of these NSs. Few microliters of the NSs dispersion in hexane were deposited onto a glass substrate. To remove the excess of organic ligands that could affect the correct estimation of thickness, the dried sample was washed twice with pure hexane. A representative AFM topography image is reported in Figure 2b. The different colors in the image correspond to different heights. From the height profiles (Figure 2c) we estimated a 3 nm thickness for a single NS, in agreement with the assessment based on the PL emission wavelength. In the height distribution over the whole AFM image

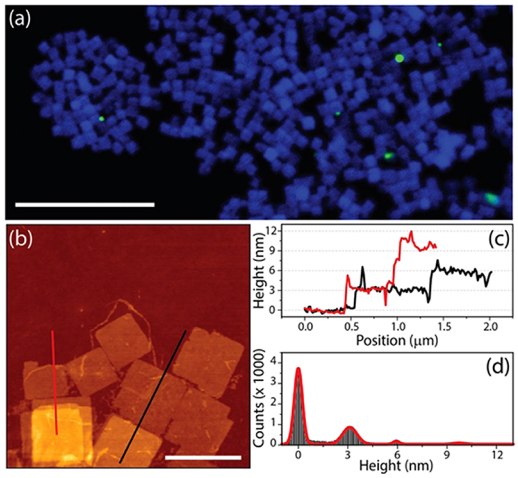

Figure 2. Confocal (a) and atomic force (b−d) microscopy analysis of the NSs. Scale bars correspond to 10 μm (panel a) and 1 μm (panel b). Panel c reports the height profiles obtained from the image in (b) along the red and black lines. (d) Height distribution over the whole image. The peak centered at 0 nm corresponds to the bare glass substrate.

(Figure 2d), apart from the peak centered at 0 nm, corresponding to the bare glass substrate, the main peak was centered at 3.1 nm, indicating a relatively monodisperse population of sheets with such thickness value. The other two minor peaks are present at approximately 6 and 10 nm, likely due to stacks of two and three NSs, respectively. It is also important to notice that the washing procedure in hexane likely removed not only the organics in excess but also most of the ligands from the surface of the NSs. Indeed, the high resolution adhesion maps as well as the maps of stiffness acquired by AFM, reported in Figure S8, indicate the presence of few small and isolated protruding features, characterized by different adhesion properties and lower stiffness with respect to the rest of the crystal plates, likely due to the presence of a few residual organic molecules.

High resolution TEM (HRTEM) and selected area electron diffraction (SAED) analyses revealed a structure matching with an orthorhombic crystal phase (ICSD 97851, a = 8.207 Å, b = 8.255 Å, c = 11.759 Å) also reported by Zhang et al. for $CsPbBr_3$ nanowires[8] and by Abhishek Swarnkar et al.[14] and Cottingham et al.[15] for $CsPbBr_3$ nanocuboids. The NSs are oriented with the zone axis [00−1] and enclosed by (110), (−1−10), (1−10), and (−110) facets (see Figure 3a). Figure 3a reports the HRTEM image of the thin area of the NS shown in the inset of the same panel, with corresponding fast Fourier transform (FFT) in Figure 3b. Data points for {210} planes (3.7 Å) are shown, which are unique for the orthorhombic phase and are missing in the cubic (ICSD 29073) and tetragonal (ICSD 109295) phases. However, some features are observed in FFTs and SAED patterns for the NSs ((100), (010), (110), (−110), (2−10) spots), which should be forbidden in kinematical diffraction conditions for orthorhombic $CsPbBr_3$, which will need further investigation. A wider view of the same nanosheet shows the presence of few nanometer-sized Pb nanoparticles, already reported for $CsPbBr_3$ nanoplatelets.[10a] Figure 3c shows the azimuthally integrated electron diffraction pattern obtained by selecting the thin area of Figure 3a, which is compared with the reference card for the said orthorhombic phase and the cubic phase formerly reported for colloidal $CsPbBr_3$ nanoplatelets (ICSD 29073).[10b] The pattern contains peaks that are unique for the orthorhombic phase (one of them is marked by an arrow).

DOI: 10.1021/jacs.6b03166
J. Am. Chem. Soc. 2016, 138, 7240−7243

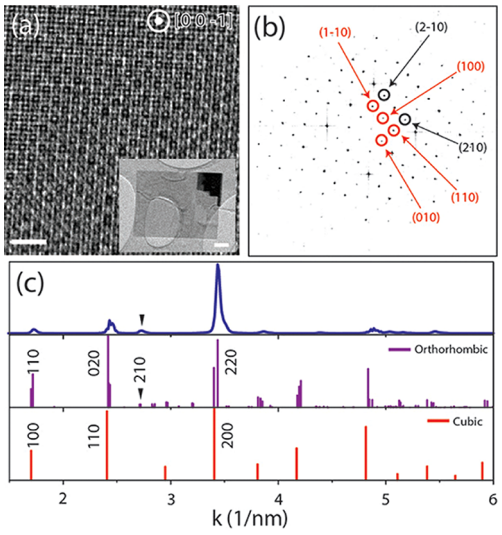

Figure 3. (a) HRTEM from a thin region of a $CsPbBr_3$ sheet partly suspended on a hole in the carbon film. Scale bar: 2 nm. The inset shows the low magnification TEM image of the whole NS. The scale bar in the inset is 100 nm. (b) Corresponding FFT of (a), consistent with an orientation along the [00−1] zone-axis. (c) Azimuthal integration of the SAED pattern performed on the thin area in (a), and comparison with reference cards for the orthorhombic and the cubic $CsPbBr_3$ phases, respectively.

Additional peaks are visible when the NSs are tilted with respect to the [001] orientation or in regions including multiple NSs (see Figures S9 and S10). NSs with various sizes share the same orthorhombic phase (see Figure S11).

In line with previous reports on anion exchange on halide perovskite nanocrystals,[10b,11,16] these NSs too could undergo anion exchange in the presence of Cl^- and I^- anions, such that they could be converted to the corresponding chloride and iodide perovskite, with preservation of shape and quantum confinement in the vertical direction (Figure S12 of the SI). In summary, we have reported the colloidal synthesis of single crystal NSs with lateral dimensions tunable up to the micron regime (this is achieved by dosing the ratio of short to long ligands in the synthesis protocol), yet with vertical size in the quantum confinement regime. The large lateral size of these sheets should make the investigation of their physical properties more affordable and should facilitate their integration in field effect transistors and photodetectors. Additionally, and unlike previous works in which large perovskite sheets were essentially not confined in the vertical direction, the influence of quantum confinement effect of the present sheets can be finally tested in devices.

■ ASSOCIATED CONTENT

Supporting Information

The Supporting Information is available free of charge on the ACS Publications website at DOI: 10.1021/jacs.6b03166.

Experimental details; TEM images and PL spectra of NSs prepared at different reaction parameter; UV−vis absorption spectra of different lateral size of $CsPbBr_3$ NSs; additional characterizations on $CsPbBr_3$ NSs; PL and TEM of Cl^- and I^- based NSs obtained through anion exchange reactions (PDF)

■ AUTHOR INFORMATION

Corresponding Authors

*mirko.prato@iit.it

*liberato.manna@iit.it

Notes

The authors declare no competing financial interest.

■ ACKNOWLEDGMENTS

We acknowledge funding from the European Union seventh Framework Programme under Grant Agreement No. 614897 (ERC Consolidator Grant "TRANS-NANO"). The authors thank Dr. M. Arciniegas for discussions.

■ REFERENCES

(1) Geim, A. K. *Science* **2009**, *324*, 1530.

(2) (a) Zhang, H. *ACS Nano* **2015**, *9*, 9451. (b) Zhao, W.; Ribeiro, R. M.; Eda, G. *Acc. Chem. Res.* **2015**, *48*, 91. (c) Ataca, C.; Şahin, H.; Ciraci, S. *J. Phys. Chem. C* **2012**, *116*, 8983. (d) Lin, Y.; Williams, T. V.; Connell, J. W. *J. Phys. Chem. Lett.* **2010**, *1*, 277.

(3) Tan, C.; Zhang, H. *Nat. Commun.* **2015**, *6*, 7873.

(4) (a) Wang, F.; Wang, Y.; Liu, Y.-H.; Morrison, P. J.; Loomis, R. A.; Buhro, W. E. *Acc. Chem. Res.* **2015**, *48*, 13. (b) Lhuillier, E.; Pedetti, S.; Ithurria, S.; Nadal, B.; Heuclin, H.; Dubertret, B. *Acc. Chem. Res.* **2015**, *48*, 22.

(5) (a) Schmidt, L. C.; Pertegás, A.; González-Carrero, S.; Malinkiewicz, O.; Agouram, S.; Mínguez Espallargas, G.; Bolink, H. J.; Galian, R. E.; Pérez-Prieto, J. *J. Am. Chem. Soc.* **2014**, *136*, 850. (b) Protesescu, L.; Yakunin, S.; Bodnarchuk, M. I.; Krieg, F.; Caputo, R.; Hendon, C. H.; Yang, R. X.; Walsh, A.; Kovalenko, M. V. *Nano Lett.* **2015**, *15*, 3692. (c) Aygüler, M. F.; Weber, M. D.; Puscher, B. M. D.; Medina, D. D.; Docampo, P.; Costa, R. D. *J. Phys. Chem. C* **2015**, *119*, 12047. (d) Zhang, F.; Zhong, H.; Chen, C.; Wu, X.-g.; Hu, X.; Huang, H.; Han, J.; Zou, B.; Dong, Y. *ACS Nano* **2015**, *9*, 4533. (e) Huang, H.; Susha, A. S.; Kershaw, S. V.; Hung, T. F.; Rogach, A. L. *Adv. Sci.* **2015**, *2*, 00194. (f) Zhu, F.; Men, L.; Guo, Y.; Zhu, Q.; Bhattacharjee, U.; Goodwin, P. M.; Petrich, J. W.; Smith, E. A.; Vela, J. *ACS Nano* **2015**, *9*, 2948. (g) Huang, H.; Zhao, F.; Liu, L.; Zhang, F.; Wu, X.-g.; Shi, L.; Zou, B.; Pei, Q.; Zhong, H. *ACS Appl. Mater. Interfaces* **2015**, *7*, 28128.

(6) (a) Sichert, J. A.; Tong, Y.; Mutz, N.; Vollmer, M.; Fischer, S.; Milowska, K. Z.; García Cortadella, R.; Nickel, B.; Cardenas-Daw, C.; Stolarczyk, J. K.; et al. *Nano Lett.* **2015**, *15*, 6521. (b) Vybornyi, O.; Yakunin, S.; Kovalenko, M. V. *Nanoscale* **2016**, *8*, 6278.

(7) Dou, L.; Wong, A. B.; Yu, Y.; Lai, M.; Kornienko, N.; Eaton, S. W.; Fu, A.; Bischak, C. G.; Ma, J.; Ding, T.; et al. *Science* **2015**, *349*, 1518.

(8) Zhang, D.; Eaton, S. W.; Yu, Y.; Dou, L.; Yang, P. *J. Am. Chem. Soc.* **2015**, *137*, 9230.

(9) Sun, S.; Yuan, D.; Xu, Y.; Wang, A.; Deng, Z. *ACS Nano* **2016**, *10*, 3648.

(10) (a) Akkerman, Q. A.; Motti, S. G.; Srimath Kandada, A. R.; Mosconi, E.; D'Innocenzo, V.; Bertoni, G.; Marras, S.; Kamino, B. A.; Miranda, L.; De Angelis, F.; et al. *J. Am. Chem. Soc.* **2016**, *138*, 1010. (b) Bekenstein, Y.; Koscher, B. A.; Eaton, S. W.; Yang, P.; Alivisatos, A. P. *J. Am. Chem. Soc.* **2015**, *137*, 16008.

(11) Akkerman, Q. A.; D'Innocenzo, V.; Accornero, S.; Scarpellini, A.; Petrozza, A.; Prato, M.; Manna, L. *J. Am. Chem. Soc.* **2015**, *137*, 10276.

(12) Yantara, N.; Bhaumik, S.; Yan, F.; Sabba, D.; Dewi, H. A.; Mathews, N.; Boix, P. P.; Demir, H. V.; Mhaisalkar, S. *J. Phys. Chem. Lett.* **2015**, *6*, 4360.

(13) Yakunin, S.; Protesescu, L.; Krieg, F.; Bodnarchuk, M. I.; Nedelcu, G.; Humer, M.; De Luca, G.; Fiebig, M.; Heiss, W.; Kovalenko, M. V. *Nat. Commun.* **2015**, *6*, 8056.

(14) Swarnkar, A.; Chulliyil, R.; Ravi, V. K.; Irfanullah, M.; Chowdhury, A.; Nag, A. *Angew. Chem., Int. Ed.* **2015**, *54*, 15424.

(15) Cottingham, P.; Brutchey, R. L. *Chem. Commun.* **2016**, *52*, 5246.

(16) Nedelcu, G.; Protesescu, L.; Yakunin, S.; Bodnarchuk, M. I.; Grotevent, M. J.; Kovalenko, M. V. *Nano Lett.* **2015**, *15*, 5635.

DOI: 10.1021/jacs.6b03166
J. Am. Chem. Soc. 2016, 138, 7240−7243